remote sensing

MDPI

Article

The Impact of Dealiasing Biases on Bird and Insect Data Products of C-Band Weather Radars and Consequences for Aeroecological Applications

Nadja Weisshaupt *, Bent Harnist and Jarmo Koistinen

Nowcasting and Intelligent Traffic Weather Research Group, Finnish Meteorological Institute, PL 503, 00101 Helsinki, Finland

* Correspondence: nadja.weisshaupt@fmi.fi

Abstract: (1) The aliasing of radial velocities from weather radars is a known challenge in meteorology. It may also occur during bird migration if the unambiguous velocity threshold is below the birds' ground speed. High variability in birds' radial velocities and high flight speeds lead to multiple aliasing (folding) and challenge meteorological dealiasing approaches. Unfolded radial velocities are essential for calculating flight directions and speed and derived migration traffic rates for aeroecological applications. (2) We study the occurrence of aliasing in measurements of different pulse repetition frequencies (PRF) in C-band weather radars in bird and insect cases and test the efficiency of a dealiasing algorithm widely used in biological weather radar software. We use dual-PRF measurements as a reference to avoid the folding of radial velocities in quantitative and qualitative bird migration outputs. (3) The dealiasing algorithm performed poorly in single-PRF measurements during bird migration, though not in insect and precipitation cases. In contrast, dual-PRF velocities yielded proper flight speeds, flight directions and migration traffic rates. (4) The study unveils severe biases in aeroecological analyses of C-band weather radars from imperfectly dealiased single-PRF radial velocities. Dual-PRF measurements with appropriate dealiasing postprocessing offer a valid alternative to single PRF and should be preferred whenever available.

Keywords: pulse repetition frequency; dealiasing; Doppler weather radar; radial velocity; migration traffic rate

Academic Editor: Gad Levy

Received: 12 November 2024
Revised: 16 January 2025
Accepted: 24 January 2025
Published: 27 January 2025

Citation: Weisshaupt, N.; Harnist, B.; Koistinen, J. The Impact of Dealiasing Biases on Bird and Insect Data Products of C-Band Weather Radars and Consequences for Aeroecological Applications. *Remote Sens.* **2025**, *17*, 436. https://doi.org/10.3390/rs17030436

1. Introduction

Recent technical and computational advances in signal interpretation and data processing have rendered weather radar (WR) data more accessible to a broader user group, e.g., [1–4]. During the development of biological WR-based software and applications, scientists have undertaken a variety of validation studies between WRs and other radar types or other monitoring approaches, e.g., [5–8]. These comparisons have revealed variable degrees of correlation between the observation systems resulting from various technological, analytical and biological causes. However, the suspected technological reasons in particular have largely remained as unverified expert guesses.

To study birds' long annual journeys, large networks of uniform radar systems, as the WR networks provide, seem ideal. However, despite their common denomination as weather radars, WRs exhibit considerable heterogeneity in system properties and consequently measurements [9,10]. Data heterogeneity challenges processing approaches and product generation across countries. In Europe, the Operational Program on the Exchange

of Weather Radar Information (OPERA) was established to foster cooperation between European countries for meteorological data exchange and enhance data product quality [11]. Vertical profiles of nocturnal passerine migration sourced from OPERA data processed by the vol2bird algorithm in the R package bioRad [2] can be nowadays downloaded from the data repository Aloft (https://aloftdata.eu/ [12]). These vertical profiles include bird density estimates, migration traffic rates (MTR), flight (ground) speeds and flight directions from WR data in Europe. The flight speeds and flight directions are derived from radial velocities (VRAD) processed by the volume velocity processing (VVP) technique [13,14]. When displayed as a function of azimuth angle (so-called Velocity-Azimuth-Display, VAD) the radial velocities of the elevation angles within the same altitude layer of a uniform motion field constitute a sine curve [15,16]. The phase angle (x-axis) of the maximum gives the birds' average flight direction and the respective amplitude (y-axis) the birds' ground speed (V_g). The VRAD residual standard deviation to a fit (sine curve) calculated using the chi-square merit function [17] serves to distinguish birds (>2 m s^{-1}) from precipitation (<2 m s^{-1}) [18]. Correct bird-only radial velocities are a prerequisite for calculating MTRs (birds km^{-1} h^{-1}), a standard estimate of migration intensity derived from ground speeds [19]:

$$\text{Migration traffic rate} = \sum_n h \times V_{gn} \times \rho_n \quad (1)$$

where V_{gn} is the birds' ground speed in km h^{-1} at altitude layer n of width h 0.2 km and ρ_n the bird density (individuals km^{-3}) at altitude layer n, respectively, estimated from reflectivity (sensu [1]). There is an alternative MTR equation considering flight directions [19] but in the present study, we use the common version without flight directions. MTRs typically serve to quantify bird fluxes at regional to continental scales [20,21].

Radial velocity-derived products are sound as long as the absolute maximum of the VAD curve of the measured targets does not exceed the maximum unambiguous or Nyquist velocity (V_{max}) determined for a given pulse repetition frequency (PRF). Radial velocities of targets exceeding this limit are folded, i.e., aliased by $\pm 2V_{max}$ m s^{-1}, and require corrective dealiasing, e.g., [14,22]. Many dealiasing approaches have been proposed assuming widespread meteorological targets with uniform direction and speed in each vertical layer (e.g., [23] and citations therein, [14,24]). However, these dealiasing methods do not work well for unevenly distributed targets [22] or targets with highly variable directions and speed between neighbouring sample bins, as found in large wind shears [25]. Similar difficulties may arise from birds [25,26]. For example, in the Finnish WR network, in which the transmission frequency is between 5.61 and 5.65 GHz (C-band), the unambiguous velocity threshold is as low as 7.6 m s^{-1} for operational measurements with a PRF of 570 Hz. As birds' air speed (potentially increased by tailwind assistance) is typically between 10–20 m s^{-1} (e.g., [27]), birds easily surpass the unambiguous velocity threshold and lead to single or even multiple velocity aliasing (simulated in Figure 1).

PRF (f_{PRF}) and Nyquist velocity (V_{max}) are inseparably intertwined through the definition [28]:

$$V_{max} = \lambda f_{PRF}/4 \quad (2)$$

where λ is the wavelength of the radar. Therefore, assuming a wavelength of 0.053 m in C-band and V_{max} of 20 m s^{-1}, PRF should be at least 1509 Hz to correctly represent most passerine migration in weak to moderate tailwinds. Such a high PRF, however, would lead to an impractically short unambiguous measurement range in operational use. For S-band, especially common in the US, the Nyquist velocity would be approximately twice as high as the one from C-band for the same PRF.

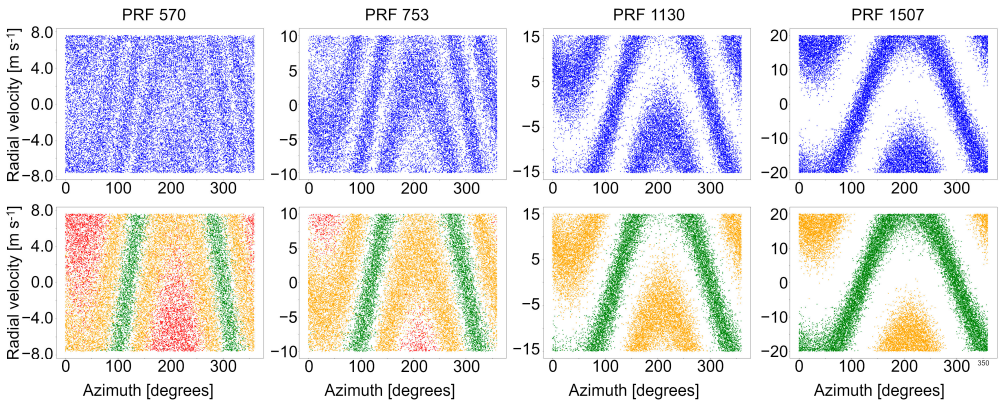

Figure 1. Aliasing cases for PRFs of 570, 753, 1130 and 1507 Hz obtained with the Gaussian velocity simulator (see Appendix A) for a ground speed of 25 m s^{-1}. Colours in the lower row indicate folding of velocity values: green: not folded; orange: folded once; red: folded twice.

The vol2bird algorithm deploys the dealiasing method developed by [29] (hereafter referred to as HL). A case study by [26] indicated deficient performance of the dealiasing algorithm in vol2bird in Finnish WR data. However, dealiasing performance has not been thoroughly assessed and the prevalence of the issue, consequences for bird products and possible solutions are unknown. Erroneous radial velocity derivates, hence, represent a potential source of serious bias in quantitative and qualitative migration analyses.

In meteorology, it was proposed to use dual-PRF velocity measurements to avoid aliasing, e.g., [14,30]. The dual-PRF technique combines two different PRFs sampled in two separated adjacent azimuthal sectors (e.g., 0.5° wide each) to extend the unambiguous velocity (e.g., to 40 m s^{-1} or more) which is defined by the unambiguous velocities of each of the two applied PRFs (V_{max1} and V_{max2}) [31]:

$$V_{max12} = (V_{max1}\ V_{max2}) / |(V_{max1} - V_{max2})| \quad (3)$$

The higher unambiguous velocities of dual-PRF sweeps seemingly represent a propitious alternative to single-PRF measurements also in biological analyses [2]. In dual-PRF measurements, the occurrence of outliers is a well-known artefact resulting from imperfect dealiasing based on the two original PRFs [32]. The theory behind the dealiasing technique is that the two PRF modes sample the same velocity despite originating from two separated adjacent azimuthal sectors. However, there are various conditions in which this assumption may be violated and consequently dealiasing fails in accordance with the heterogeneity of the measured radial velocities in the neighbouring atmospheric sample bins. This leads to various amounts of radial velocity outliers, e.g., [25,33] (Figure 2). The positive or negative velocity error of these outliers is approximately twice the low or high unambiguous velocity from the centre of the main velocity sinusoid [25].

Ref. [18] found outlier fractions in dual-PRF velocities of birds to be 15% and 1% for precipitation. They remove outliers "during the VVP analysis by an iterative fitting procedure" applying an exclusion threshold of 10 m s^{-1} from the first velocity fit. There is no mention of aliased outliers. For vol2bird, ref. [2] recommend no dealiasing for dual-PRF measurements because dual-PRF velocities are "dealiased at acquisition time".

Even though various postprocessing algorithms for dealiasing or outlier removal have been developed for single and dual PRF, they typically serve as in-house postprocessing in meteorological institutes and are not applied to data shared, e.g., through OPERA, or for use in aeroecology.

While aliasing is a known challenge in WR-based bird migration analyses, it is unknown if and to what extent insects can be affected by it and if there might be similar

challenges with dealiasing algorithms. As insects are typically transported by winds with low or no own flight speed contribution, e.g., [34,35], the probability of aliasing could be expected to be low or like the one of precipitation. In addition, insects would largely move as uniformly as precipitation and therefore meteorological dealiasing approaches could be assumed to be equally successful as in precipitation. However, we are not aware of studies on insect velocity aliasing in WR data.

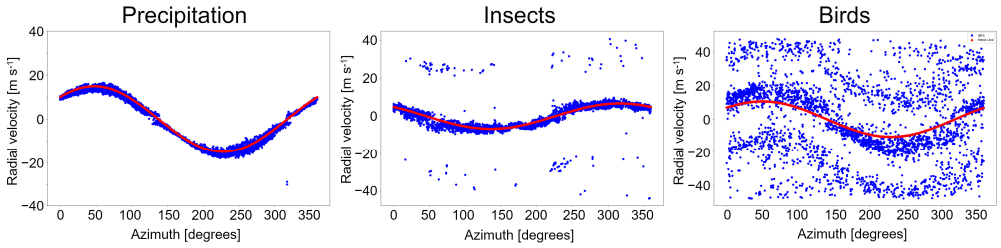

Figure 2. Examples of dual-PRF radial velocities (blue dots) and their respective sine fit curve (red line) from the Kankaanpää radar as VAD: precipitation (**left**) with two outliers on 11 October 2023 7 am UTC, insects (**centre**) with several outliers on 5 June 2024 9 am UTC and birds (**right**) with partly aliased outlier sidebands on 29 April 2024 8 pm UTC.

In this study, we investigate the impact of different PRFs on velocity measurements, which are an indispensable component in the calculation of MTRs from WR data widely used in bird migration studies. We hypothesize that differences in flight directions and speeds, and especially MTRs found in calibration studies between WRs, may be in part explained by radial velocity quality and the performance of dealiasing approaches. We compare bird- and insect-dominated measurements of four single PRFs to dual PRF and support our findings by radial velocity simulations. We further discuss the quality of dual-PRF velocities and related challenges in bird, insect and precipitation cases as well as potential effects and artefacts in radial velocity-derived products and suggest solutions to overcome dual-PRF biases.

2. Materials and Methods

2.1. Birds

2.1.1. Radar Data

Radar observations were sourced from 10 Finnish polarimetric C-band weather radars (WRM200, Vaisala, Helsinki, Finland; Figure 3).

In long-range scanning, the Finnish WR network operates at a single PRF of 570 Hz at six elevation angles over 0.3° to 9.0°. Dual-PRF velocities are operationally sampled at an elevation angle of 2° and 7°. The dual PRF uses 900 and 1200 Hz. Applying this setting in Equation (3) above, with V_{max1} = 11.93 m s^{-1}, and V_{max2} = 15.90 m s^{-1}, we obtain a maximum unambiguous dual-PRF velocity V_{max12} of 48 m s^{-1} (Table 1).

Table 1. Pulse repetition frequencies (PRF) used in the present study (Hz) and their respective Nyquist velocities (V_{max}) in m s^{-1}. The Nyquist velocities of the two PRFs constituting the dual PRF are given in brackets.

			Single PRF		**Dual PRF**
PRF [Hz]	570	753	1130	1507	900/1200
Nyquist velocity [m s^{-1}]	7.6	10	15	20	48 (11.93, 15.90)
Pulse length [μs]	2.0	1.0	0.8	0.5	-

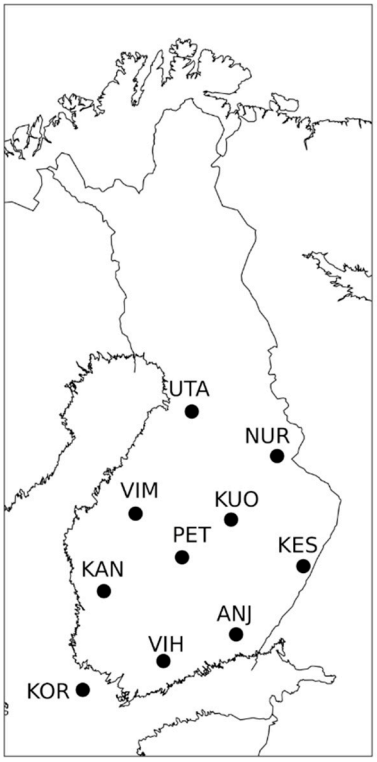

Figure 3. Location of the Finnish C-band weather radars used in the present study: Anjalankoski (ANJ), Kankaanpää (KAN), Kesälahti (KES), Korppoo (KOR), Kuopio (KUO), Nurmes (NUR), Petäjävesi (PET), Utajärvi (UTA), Vihti (VIH), Vimpeli (VIM).

For this study, we added measurements with three different PRFs (753, 1130 and 1507 Hz) at an elevation angle of 0.7° in the Kankaanpää weather radar ("KAN" in Figure 3, 61.8108N, 22.502E) between 10 September–30 October 2023 and 10 April–10 June 2024. For simplicity, we refer to the different PRFs as PRF 570, PRF 753 and so on. The maximum unambiguous velocities of the single-PRF measurements are listed in Table 1.

Dual-PRF measurements were collected from the elevation angle at 2° for the same two periods from the Kankaanpää radar and additionally from 1–30 September 2022 from all 10 weather radars. The three periods coincide with the migration season of birds and partly with the occurrence of insects.

On each day we picked one measurement during peak activity of nocturnal passerine migration, typically between two hours after sunset and midnight local time. We selected cases with birds only to exclude potential bias from non-biological or mixed bird-insect phenomena. Cases were visually verified based on echo characteristics in the relevant polarimetric radar moments. We obtained 12 days from 2023 and 16 days from 2024 for the customized PRF measurements.

As a reference dataset based on single-PRF velocities dealiased by the HL algorithm, we downloaded vertical profiles of birds (VPBs) processed by the vol2bird algorithm [2] from the Aloft data repository (https://aloftdata.eu) for the same 10 radars in September 2022, and for the Kankaanpää radar from 10 September to 30 October 2023 and 10 April to 10 June 2024.

2.1.2. Data Preparation

Single- and Dual-PRF Velocities

To check the extent of aliasing and the performance of the HL algorithm in different single PRFs in biological cases, we implemented the HL algorithm in our velocity analyses. By applying the Velocity Azimuth Display (VAD) technique [36], we determined birds'

flight speeds (amplitude) and directions (angle) from the phase maximum for radial VAD-velocities of the four single-PRF modes in untreated and dealiased (by the HL algorithm) form at the elevation angle of 0.7°. We selected the height layer of 400–600 m for comparison as it would typically contain more birds than the lower and the higher layers. An example of radial velocities of each of the PRF modes is shown in Figure 4. The outer range of the annular bird echo pattern becomes narrower with increasing single PRF which is due to shorter pulse lengths with increasing PRF compared to PRF 570 leading to lower sensitivities of 6–12 dB and thus a shorter detection range (Table 1). We discarded single-PRF cases with a residual standard deviation below 2 m s^{-1} mimicking the filter mechanism of vol2bird [2].

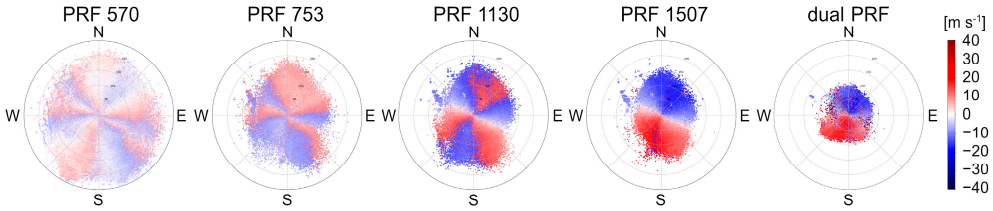

Figure 4. Untreated radial velocities in five PRF modes on 5 October 2023 at elevation 0.7°. From left to right: 570, 753, 1130 and 1507 Hz and dual PRF. Aliasing can be seen in PRF 570, 753 and 1130, while PRF 1507 and dual PRF show almost unfolded radial velocities. In dual PRF, the outliers cause some inconsistencies in the texture of the velocity field.

To test the difference between birds' flight speeds and directions from untreated dual PRF and quality-controlled dual PRF and to use them as a reference for single PRFs, we employed untreated dual-PRF velocities on the one hand and, on the other, we developed a bird-specific outlier correction for dual-PRF velocities which includes two sine fits and the correction of aliased sidebands (exemplified by a case of bird migration in Figure 5).

In the first step, we identified and extracted bird bins by the Naïve Bayes classifier by [4] to constitute our input data. As the classifier was implemented at the Finnish Meteorological Institute for single-PRF measurements only, there was no classification available at the dual-PRF elevation angle of 2°. We therefore combined bin-based polarimetric classification from neighbouring single-PRF elevation angles (1.5° and 3°) with dual-PRF measurements in 200-m altitude layers [26]. That is, the non-classified dual-PRF velocity data were sampled in the volume between the single-PRF measurements classified according to [4] (Figure S1). This setting of interleaved elevations is suitable for spatially extensive and uniform migrations, such as nocturnal passerine migration. The motion field can be assumed to be uniform between the elevations of 1.5 and 3° given there are no significant geographical barriers deviating migration. (If echo classification were run for dual-PRF measurements, these could be directly taken from the same bins as radial velocities at 2°). Dual-PRF velocities were approved if the mean bird probabilities of the 1.5° and 3° single-PRF measurement from the bins within the same azimuth and 200-m altitude layer was at least 50%, i.e., the dominant class. The dual-PRF bins in the azimuths that passed this selection were then included in the dealiasing treatment of outliers as follows.

Outliers in sidebands are symmetrically arranged on both sides of the main radial velocity sinusoid at a distance of the approximate sum of the unambiguous velocity of each PRF mode applied (as defined in Equation (2)) (Figure 5). With PRFs of 900 and 1200 Hz this gives an approximate distance of ±23.85 or ±31.80 m s^{-1} from the centre of the main sinusoid obtained by a VAD estimate fit. Aliased sideband outliers are typically located as isolated velocity measurements outside the range of the sidebands on the opposite side of the absolute maximum amplitude (Figure 5), similar to single-PRF aliasing in Figure 1. To correct aliasing of outliers, our outlier algorithm first made a VAD fit on the complete

original velocity estimates including all data points. Then, we set a piecewise continuous function as a buffer for acceptable outliers at 35 m s^{-1} from the first VAD estimate fit, which takes into account natural variability in the velocity measurements. All data points outside the buffer were shifted by the unambiguous velocity of the dual PRF to the opposite side of the first sine fit curve from their current location, i.e., either −48 m s^{-1}, if situated opposite the negative values of the sine fit curve and outlier $V_r > 0$, or +48 m s^{-1}, if located opposite the positive values of the sine fit curve and outlier $V_r < 0$, with no shift at zero amplitude. Tighter thresholds, e.g., 10 m s^{-1} for sideband removal as proposed by [18], may cut out parts of the main bird sine curve and retain parts of sidebands, especially in cases of sideband aliasing when the first fit can be far from the main sine curve as in Figure 5. Finally, a corrected VAD fit was made using the corrected data yielding flight speeds and flight directions in 200-m height layers as described above. Flight estimates were approved based on three conditions: (1) the VAD contained at least 500 radial velocity measurements, (2) the proportion of bird bins (with a probability of at least 50%) versus all velocity bins in each altitude layer of 200 m was at least 70%, and (3) flight speed was at least 7 m s^{-1}. These quality thresholds were defined based on previous visual inspection of the velocity data in all dual-PRF cases. This approach proved to be robust in cases of both aliasing and non-aliasing. The proportion of outliers relative to the overall number of radial velocity measurements may help identify bird cases if other classifications are unavailable.

From these quality-controlled dual-PRF velocities, we derived respective bird flight speeds and directions. Dual-PRF MTRs were calculated based on Equation (1) integrating the bird densities and flight speeds obtained from the classified bins.

Dual-PRF velocities were not fed into the HL dealiasing algorithm because the algorithm would render them chaotic in bird cases as they do not correspond to the one-curve pattern expected for the HL algorithm.

We label outcomes as "dealiased" irrespective of dealiasing quality.

Animal Densities

For estimating animal densities, radar samples were processed by the Naïve Bayesian classifier by [4] which provides bin-based probabilities of 19 target classes, including birds and insects. Based on these probabilities, bird or insect bins were selected (or discarded) to constitute the bird or insect data pool. Using the classified bins with a minimum probability of 50% for the respective class, mean insect or bird densities per 200-m height layer were estimated from radar reflectivities sensu [1] between a height interval of 0–1 km in a radius of 5–40 km around each radar and from six elevation angles between 0.3° and 9°. Bird densities were used to estimate MTRs following Equation (1). The limited height interval was chosen to focus on layers with maximum bird concentration and thus the best data. Low bird densities can affect sine curve fitting and therefore affect the calculation of MTRs.

2.1.3. Data Analysis

All analyses and visualisations of Finnish WR data were executed in Python version 3.12 [37] and R version 4.2.2 [38]. Vertical profiles of birds were processed with the R package bioRad [2].

Comparison of PRF Modes

We calculated the proportion of flight speeds in the height layer of 400–600 m and MTRs between 0 and 1 km for each single-PRF mode and as a reference flight speeds and MTRs from dual PRF without outlier correction (referred to as "dual PRF") and dual PRF with outlier correction including classified bird bins as described above (hereafter "dual PRF FMI"). We computed the circular mean of aliased and dealiased flight directions for each single-PRF mode per selected season in the height layer of 400–600 m.

Dual-PRF Outliers

To assess the impact of outliers on birds' and insects' flight speeds and directions, we compared flight speeds and directions from measured dual-PRF radial velocities before (i.e., untreated data) and after (i.e., dealiased data) outlier (sideband) correction. We calculated the differences between the flight speeds and directions as well as means, residual standard deviations and confidence intervals of the untreated and dealiased radial velocities. We also simulated the impact of outlier aliasing on sine fit for a mean flight speed of 25 m s^{-1} and variable proportions of outliers relative to overall velocity data points (see Appendix A). We calculated fractions of outliers of bird, insect and precipitation cases in 200-m height layers between 0–1 km from 2023 and 2024 applying a threshold of 10 m s^{-1} from the second sine fit curve.

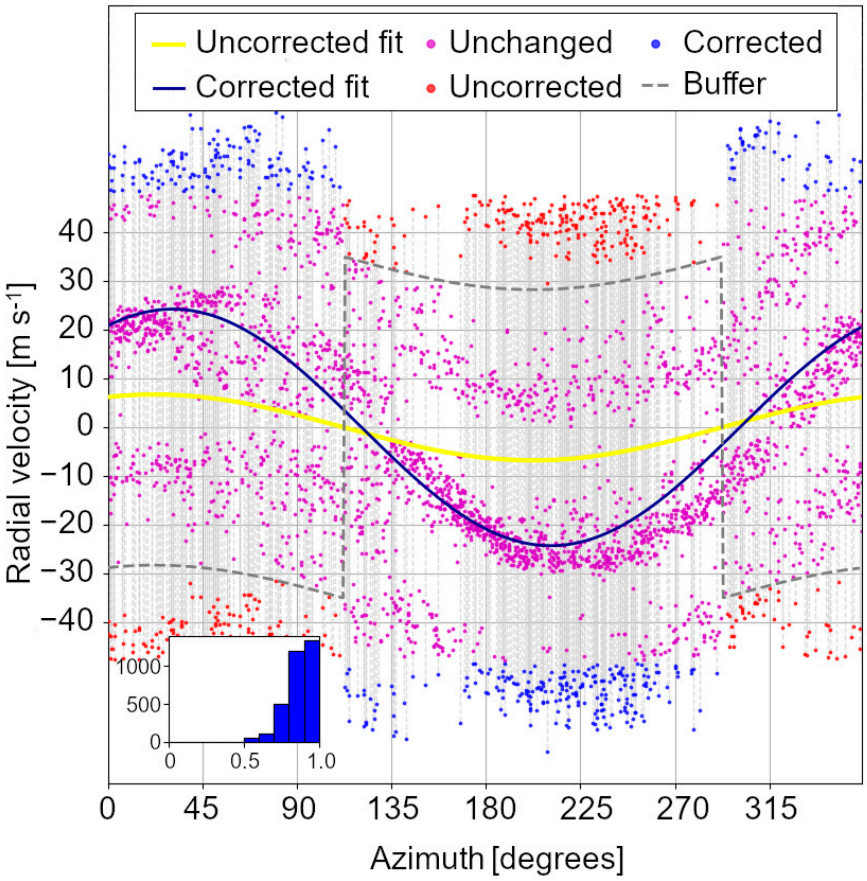

Figure 5. Dual-PRF radial velocity with outlier sidebands and sine curve fits before (yellow curve) and after (blue curve) outlier aliasing correction in a case of bird migration in the height layer of 400–600 m on 29 April 2024 at 1 am UTC. Purple dots are non-aliased velocity measurements (regular and outliers) and the red ones aliased outliers shifted to the dealiased positions indicated by blue dots. The grey dotted line denotes the buffer of 35 m s^{-1} set to define outliers to be shifted. The inset shows a histogram of the probabilities of the targets in each velocity bin being birds, as determined by the classification algorithm of [4].

2.2. Insects

Insect-only cases were extracted from the same radars between sunrise and sunset from the same periods in 2023 and 2024 as the bird cases. This yielded data from 7 days in 2023 and 12 days in 2024. Extraction of insect flight speeds and directions followed the same VAD procedure as the one for birds in the height layer of 400–600 m. We compared radial velocity patterns and directions between single PRFs (570, 753, 1130 and 1507 Hz) and dual PRF (with no outlier correction) without involving vol2bird which is designed for

bird analyses. We calculated residual standard deviations of dual-PRF velocities in insect cases prior to outlier treatment to assess its potential as a filter threshold between birds, insects and precipitation.

2.3. Precipitation Cases

We randomly collected 12 cases of widespread rain and 13 cases of convective rain from spring to autumn in 2023 and 2024 to assess dual-PRF velocity features and the impact of outliers on the residual standard deviations in five height layers of 200 m between 0–1 km. To be able to collect enough precipitation examples and as precipitation hampers movements and detection of birds and insects, precipitation cases were not necessarily selected on the same days as insect and bird cases.

2.4. Comparison of vol2bird and FMI Methodology

To compare the outcomes from the dual-PRF alternative with outlier correction and the vol2bird data based on single PRF dealiased by the HL algorithm, we calculated MTRs and bird densities at heights between 0–1 km where velocity measurements are most abundantly available. As low bird densities may be linked with poor flight directions in vol2bird (i.e., less than 5–10 birds km^{-3} [17]) and thus inherently with poor flight velocities, we removed layers with bird densities of less than 5 birds km^{-3}. We calculated Spearman's rank correlation coefficients and fitted linear regression models to MTRs for autumn 2022 and 2023 and spring 2024 for both methods.

To compare radial velocity quality, we calculated the difference between vol2bird single-PRF and FMI dual-PRF flight speeds. We furthermore visualized the flight speeds of both datasets pooling the three study periods.

3. Results

3.1. Single PRF

3.1.1. Birds

Generally, aliasing bias was inversely correlated with pulse repetition frequencies. Flight speeds typically increased after dealiasing treatment in 2023 and 2024 (Table 2). The effect was largest in the PRFs of 570, 753 and 1130 Hz where speeds approximately doubled. However, especially flight speeds from PRF 570 and 753 were still considerably lower than those of the other PRFs and the reference speed of dual PRF. PRF 1507 deviated about 5–30% from dual PRF. There was also a difference of about 20–50% between the dual-PRF speed obtained without outlier correction and the PRF with outlier correction ("dual PRF FMI"). The single-PRF measurement of 1507 Hz produced higher flight speeds than the dual-PRF measurement without outlier correction (i.e., ratios above 1) since the latter underestimates the real speed of the migrants, see below (Figure 5, Table 2).

Ratios of flight speeds of single PRFs and dual PRF with outlier correction showed a similar gradient towards improving ratios with increasing PRF as dual PRF without outlier correction. One can easily perceive from radial velocity plots of PRF 570 before and after dealiasing treatment (Figure 6a,b) that the HL algorithm could not appropriately dealias velocities but rather shifted the entire radial velocity blend into some kind of wave causing an arbitrary increase in flight speeds.

Differences between dealiased and untreated mean flight directions were pronounced in the PRFs 570 and 753, while those of PRF 1130 and 1507 pointed approximately in the same direction (Figure 7).

Table 2. Mean ratios of flight speeds in the altitude layer of 400–600 m from four single-PRF measurements relative to dual PRF without outlier correction ("dual PRF") before ("untreated") and after ("HL") dealiasing by the HL algorithm in autumn 2023 (n = 19) and spring 2024 (n = 30) and the same PRF measurements compared to the dual PRF with outlier correction ("dual PRF FMI"), n = 12 in autumn 2023 and n = 11 in spring 2024.

PRF Mode	Autumn 2023		Spring 2024	
	untreated	HL	untreated	HL
570/dual PRF	0.11	0.30	0.10	0.15
753/dual PRF	0.25	0.60	0.30	0.52
1130/dual PRF	0.64	1.10	0.75	1.16
1507/dual PRF	0.95	1.19	1.11	1.32
570/dual PRF FMI	0.07	0.25	0.06	0.10
753/dual PRF FMI	0.17	0.50	0.18	0.31
1130/dual PRF FMI	0.49	0.90	0.45	0.70
1507/dual PRF FMI	0.78	0.96	0.64	0.67
Dual PRF/dual PRF FMI	0.83	-	0.56	-

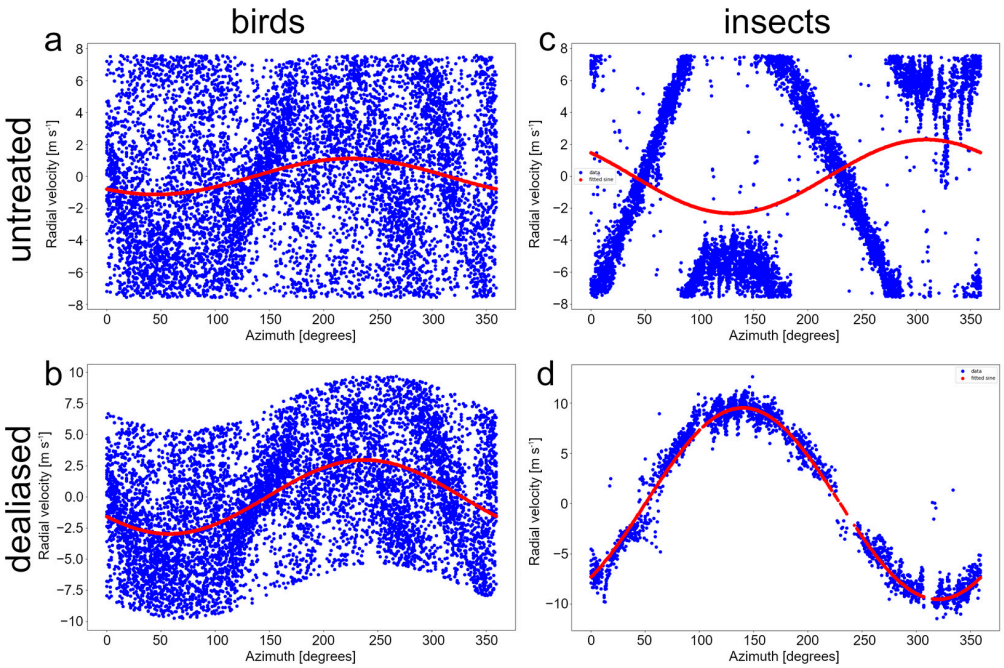

Figure 6. Examples of sine fitting in the height layer 400–600 m in single PRF 570 in birds and insects before (**a**,**c**) and after (**b**,**d**) treatment by the HL dealiasing algorithm from the Kankaanpää radar on 14 September 2023 at 8 pm UTC and 17 September 2023 2 pm UTC, respectively.

3.1.2. Insects

Aliased velocities occurred especially in low PRF measurements, in 47% of the PRF 570 cases, in 21% of PRF 753, in 0.5% of PRF 1130 and in 0% in PRF 1507 and dual PRF in 2023 and 2024 (n = 19). We did not observe multiple aliasing in insect cases. The HL algorithm was able to correct almost all aliased cases successfully, so that the different PRFs produced highly similar flight speeds and directions (Table 3, Figure 6c,d, Figures 8 and S2). Generally, risk of aliasing increased with higher altitudes, especially from 400–600 m upwards in PRF 570.

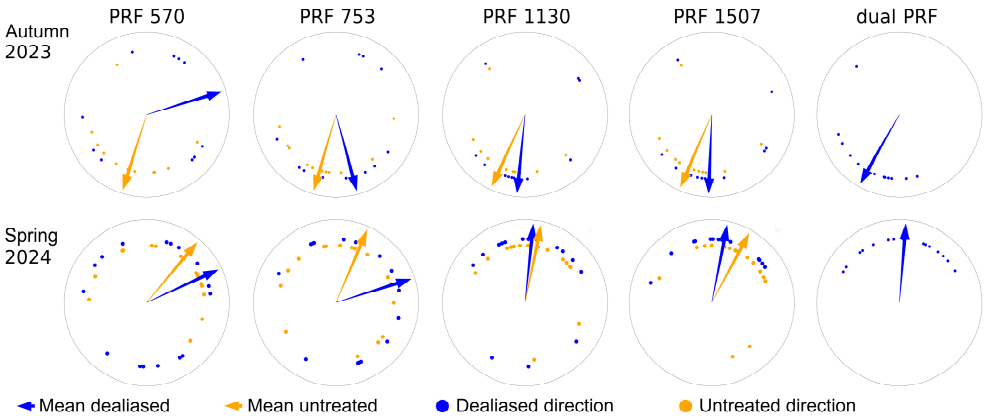

Figure 7. Flight directions of birds of PRF 570, 753, 1130, 1507 untreated (orange) and dealiased (blue) by the HL dealiasing algorithm and dual PRF with outlier correction, with the arrows indicating the circular mean flight direction of the respective processing in autumn 2023 and spring 2024.

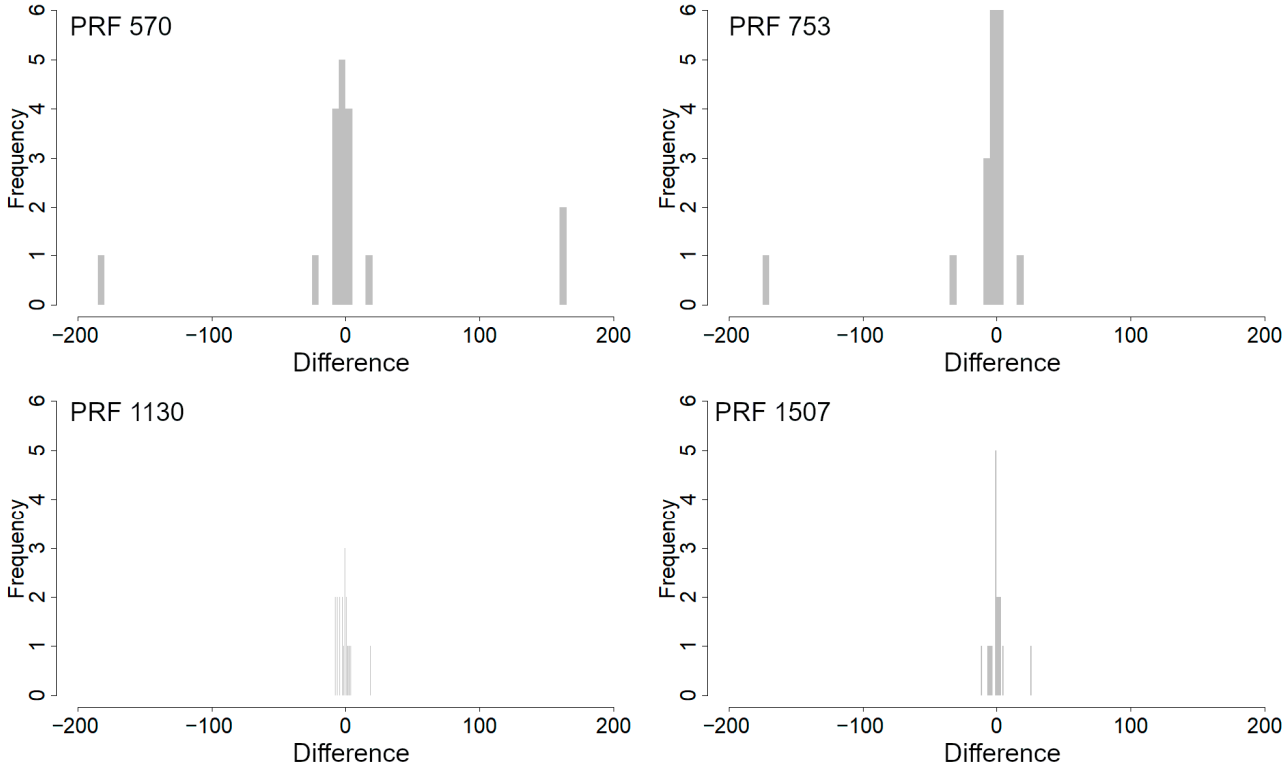

Figure 8. Differences (in degrees) between untreated and dealiased (by the HL algorithm) flight directions of insects of PRF 570, 753, 1130 and 1507 from autumn 2023 and spring 2024.

Table 3. Mean ratios of insect flight speeds in the altitude layer of 400–600 m from four single-PRF measurements relative to untreated dual PRF before ("untreated") and after ("HL") dealiasing by the HL algorithm in autumn 2023 (n = 7) and spring 2024 (n = 12).

PRF Mode	Autumn 2023		Spring 2024	
	untreated	HL	untreated	HL
570/dual PRF	0.53	1.01	0.54	0.89
753/dual PRF	0.76	1.01	0.96	1.04
1130/dual PRF	0.94	1.01	0.89	0.97
1507/dual PRF	0.91	1.01	0.97	0.99

3.2. Dual PRF

3.2.1. Simulations

Aliasing simulations with variable outlier proportions and flight speed-induced aliasing exhibited a negligible impact on flight directions. However, flight speeds were severely affected even by minor aliasing leading to errors of several meters per second. Outlier proportion per se without aliasing had only a minor impact on flight speeds (Figure 9).

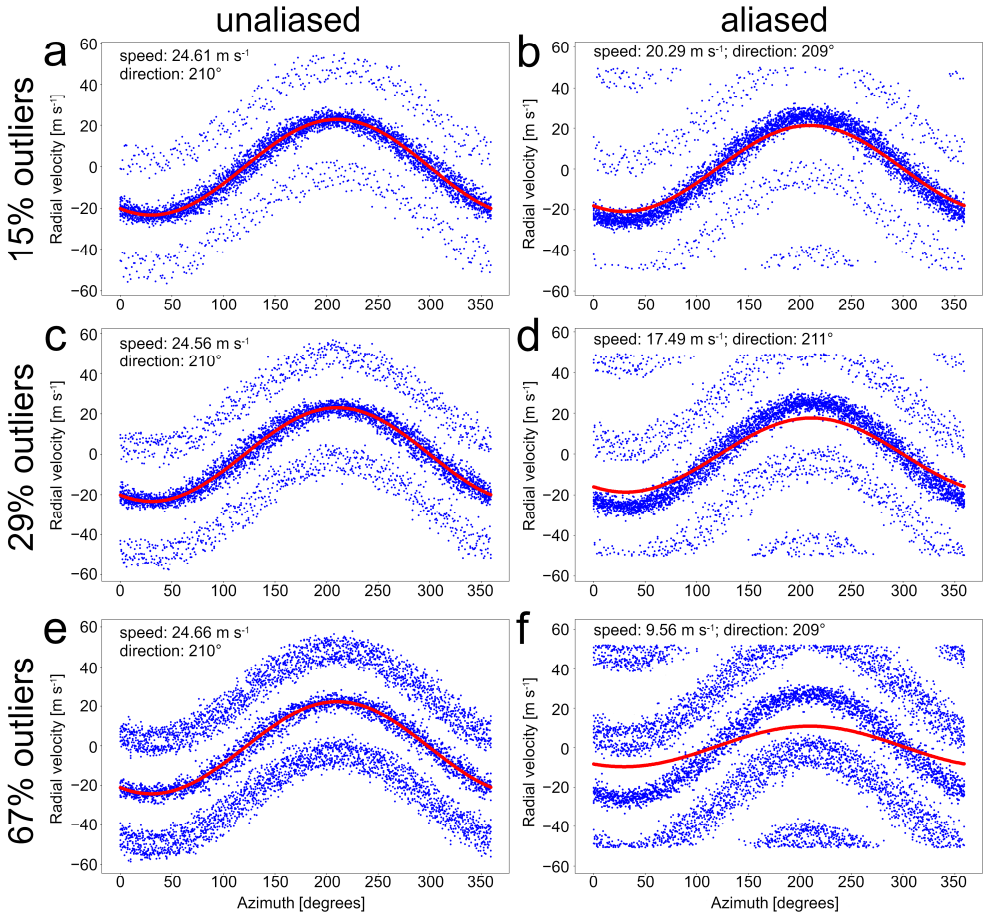

Figure 9. Simulations of dual-PRF radial velocities (blue dots) assuming a constant flight speed of 25 m s^{-1} and a proportion of 15% (**a**,**b**), 29% (**c**,**d**) and 67% (**e**,**f**) of outliers with unaliased (left column) and aliased (assuming a Nyquist velocity of 48 m s^{-1}; right column) sidebands and their effect on sine fit curves (red) and derived speeds.

3.2.2. Birds

Mean fraction of outliers in bird radial velocities was 0.30 (±0.13; 95% CI [0.29, 0.32], n = 245) of all years (Figure 10).

Analysis of dual-PRF sine fits before and after outlier correction showed a mean increase in derived flight speeds of 3.79 m s^{-1} (±3.16), with a maximum increase of 18 m s^{-1} after outlier correction. In line with simulations, differences in flight speeds before and after outlier correction grew with increasing aliasing of sidebands. Aliasing of sidebands occurred in 20% of the bird cases in 2023 and 2024. Flight directions were less prone to bias from aliasing. Directions between first and second fit varied on average by 5.53° (±10.95°). Dual-PRF velocities with outliers showed a residual standard deviation (sensu [17]) between 8.06–25.15 (mean 16.64 m s^{-1}, n = 245) in bird cases.

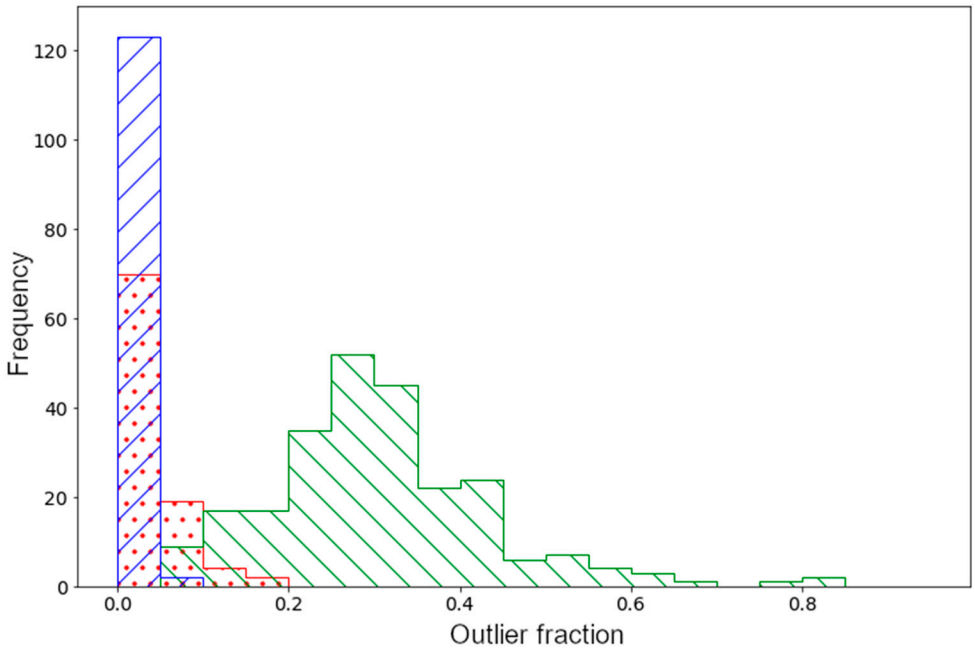

Figure 10. Fractions of bird (green, n = 245), insect (red, n = 95) and precipitation (blue, n = 125) outliers in dual-PRF measurements with a threshold of 10 m s^{-1} from the sine fit of the radial velocities in 200-m height layers between 0–1 km from 2023 and 2024.

3.2.3. Insects

Insect cases in dual PRF showed minor velocity bias resulting from the outliers. The mean dual-PRF outlier fraction in insect cases was 0.04 (95% CI [0.03, 0.05], n = 95, Figure 10). Insect flight speeds varied on average by 0.27 m s^{-1} ($\pm$ 0.32 m s^{-1}) between the first and the second VAD fit after outlier correction. Directions varied on average by 1.22° ($\pm$ 2.02°) between the first and the second VAD fit after outlier correction. Residual standard deviations ranged from 2.42–11.67 m s^{-1} (mean 5.96 m s^{-1}) in untreated insect cases.

3.2.4. Precipitation

Mean outlier proportion was 0.007 (95% CI [0.005, 0.010], n = 125) in 400–600 m (Figure 10). Mean residual standard deviation of dual-PRF radial velocities in convective rain was 3.45 m s^{-1} (95% CI [3.064 3.829], n = 65) and in widespread rain 1.69 m s^{-1} (95% CI [1.536, 1.836], n = 60) considering all height layers from 0–1 km.

3.3. Comparison of the Dual-PRF FMI Methodology with Single-PRF vol2bird

The comparison of the bird densities between the dual-PRF (FMI) and single-PRF (vol2bird) methodology in the height range of 0–1 km showed that vol2bird densities were on average 1.24 times larger (SD $\pm$ 0.66, n = 315) than the FMI densities when pooling all three years. Dual-PRF-derived MTRs were mostly larger than single-PRF MTRs from vol2bird which was particularly striking in the 2022 data (Figures S3 and S4). The correlation analysis of the MTRs between 0–1 km between the FMI and vol2bird methodology showed overall intermediate to strong correlations with a Spearman's rho of 0.65–0.97 (Table 4).

However, r-squared was modest for Kankaanpää (0.37) and particularly for the Utajärvi radar (0.20) because of several pronounced peaks not reflected in single PRF (Figure S3). A closer inspection of the Utajärvi peaks revealed rather strong migration on 17 Sept and additionally some showers east of the radar on 18 Sept and very strong migration on 20, 24 and 28 Sept. Even though vol2bird produced somewhat higher bird densities than the FMI

approach, single PRF consistently showed substantially lower flight speeds compared to dual PRF (Table S1).

Table 4. Correlation statistics for the comparison of the migration traffic rates of the dual-PRF (FMI) methodology and single-PRF (vol2bird) algorithm in the height layer of 0–1 km from 2022, 2023 and 2024. R-squared, Spearman's rank correlation coefficient, F-statistic, *p*-values and sample sizes *n* for each season and weather radar.

Year	Radar Site	Spearman's rho	F	R^2	*p*-Value	*n*
2022	Anjalankoski	0.93	135.79	0.83	<0.001	30
	Kankaanpää	0.85	8.87	0.37	<0.001	17
	Kesälahti	0.91	225.61	0.89	<0.001	30
	Korppoo	0.84	133.66	0.83	<0.001	30
	Kuopio	0.94	52.66	0.65	<0.001	30
	Nurmes	0.87	100.87	0.78	<0.001	30
	Petäjävesi	0.65	31.79	0.53	<0.001	30
	Utajärvi	0.82	7.09	0.20	<0.001	30
	Vihti	0.79	40.67	0.59	<0.001	30
	Vimpeli	0.90	134.96	0.83	<0.001	30
2023	Kankaanpää	0.97	114.56	0.92	<0.001	12
2024	Kankaanpää	0.73	46.08	0.77	<0.001	16

Flight speed analysis showed generally smaller values for the single-PRF (vol2bird) flight speeds compared to the FMI dual-PRF flight speeds in the flight speed histogram (Figure 11a) and a skewed distribution in the histogram with the differences between single-PRF (vol2bird) and dual-PRF speeds (Figure 11b) indicating smaller flight speeds in single compared to dual PRF. Medians of single- and dual-PRF flight speeds were 9.58 m s^{-1} and 14.17 m s^{-1}, respectively.

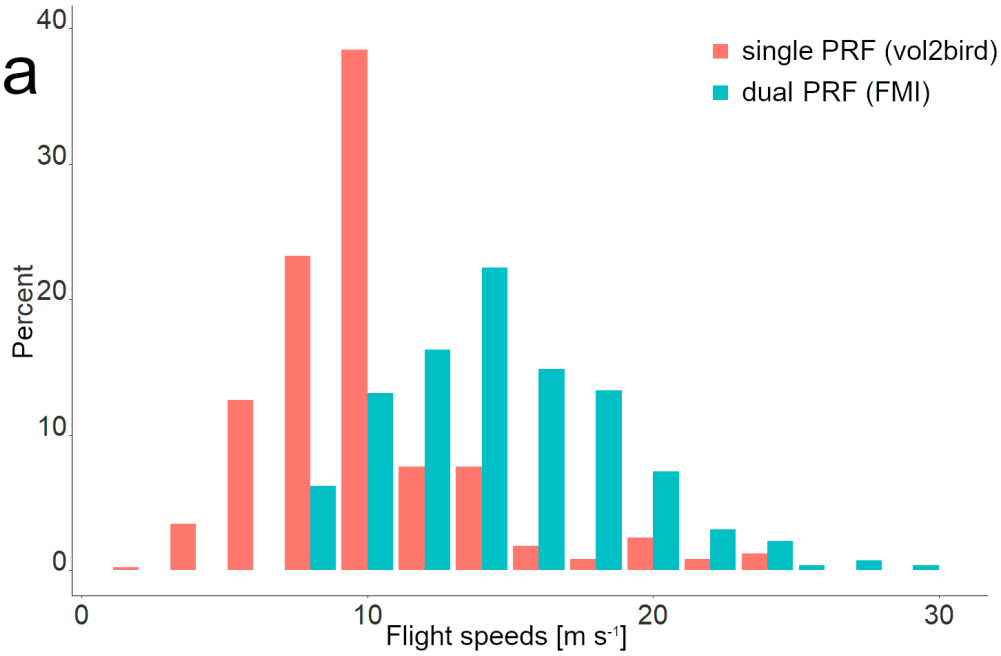

Figure 11. *Cont.*

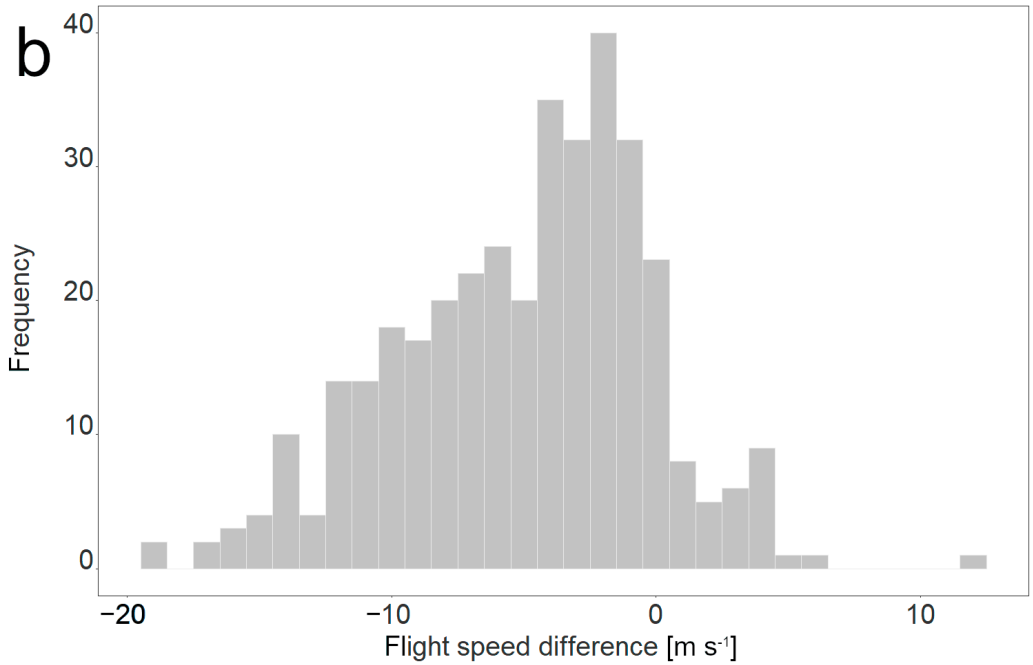

Figure 11. (**a**–**c**): Changes in mechanical properties with solution pH. (**a**) Ionically complexed IPNs show large improvements in failure stress and failure strain at intermediate pH, the failure properties are improved in comparison to the uncomplexed state. IPNs of PAAm/PNVF and PNVF/PAAm were partially hydrolyzed to PVAm/PAAc (blue closed symbols) and PAAc/PVAm (red open symbols).

Flight directions between 0–1 km showed a rather random pattern in both spring and autumn in single PRF (vol2bird), even though a certain tendency towards northwest and south can be discerned. Dual-PRF directions exhibited a clearer directional pattern to the southwest in autumn and to the north in spring (Figure 12).

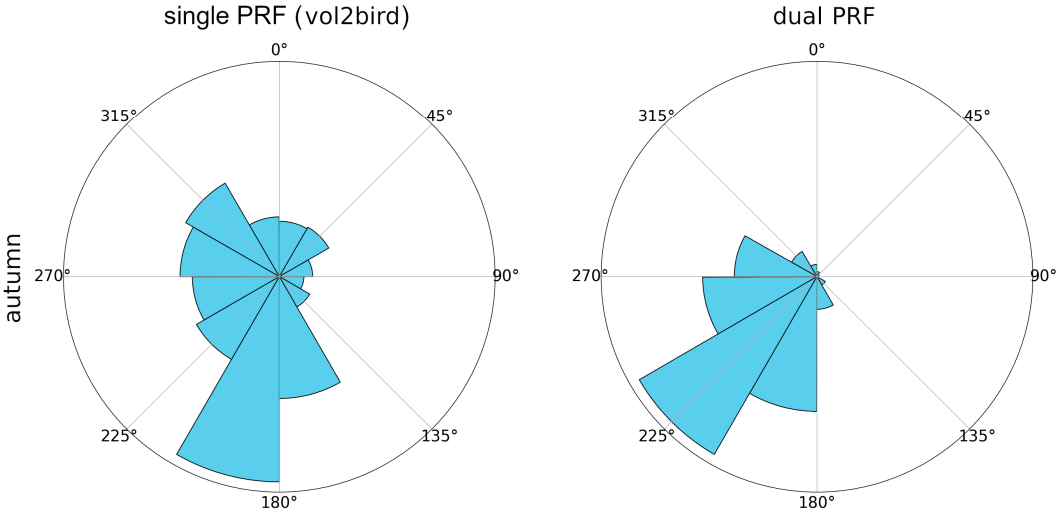

Figure 12. *Cont.*

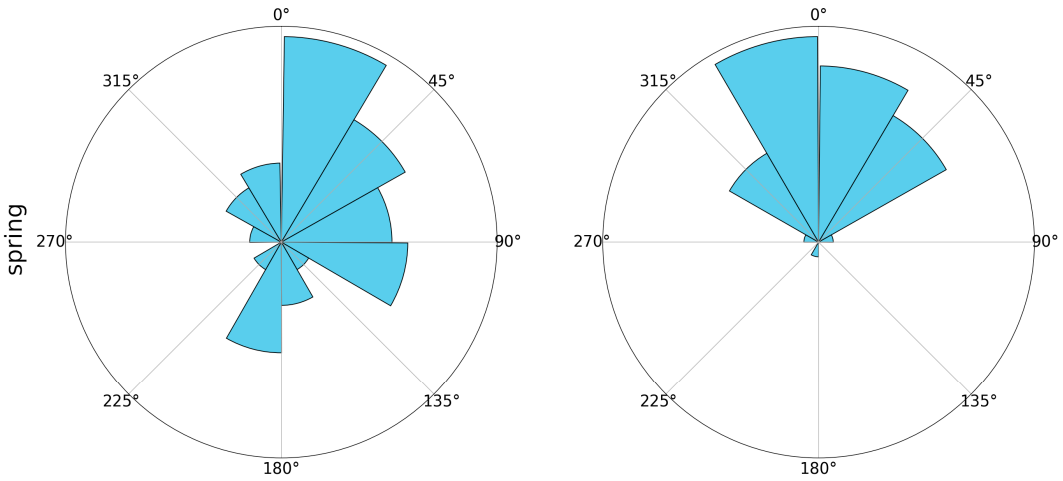

Figure 12. Flight directions between 0–1 km obtained by single-PRF (vol2bird, left column) and dual PRF (FMI, right column) methodology for autumn 2022–2023 (upper row, vol2bird n = 1119, dual PRF n = 518) and spring 2024 (lower row, vol2bird n = 63, dual PRF n = 46) samples.

4. Discussion

The analysis revealed considerable differences between PRF modes and novel insights into the performance and role of dealiasing in bird, insect and precipitation cases.

4.1. Single PRF

4.1.1. Birds

Flight speeds markedly varied between the different PRF modes, especially in the lower PRF range. The dealiasing algorithm by [29] was not able to adequately correct multiple aliasing during bird migration as typically occurs in PRF 570 and partly in 753. The main reason for the failure is the mixture of 0–2 times aliased data points and large scatter relative to the Nyquist velocity among the measured VRAD samples. Dealiasing caused a wave-like shape of the plotted radial velocities, which in turn increased the sine fit amplitude, leading to seemingly corrected or at least improved flight speeds (exemplified in Figure 6a,b). However, this meandering velocity composite does not represent a proper velocity fit as it had not reconstructed the actual clean sine curve. Flight speeds from PRF 570 were still only about 20–30% and 753 PRF only about 50% of those estimated by dual PRF. We can exclude malfunctioning of our HL algorithm as it worked fine in precipitation and insect cases exhibiting less VRAD variability. Importantly, the poor quality of flight speeds will translate into poor MTRs with the same error magnitude as flight speeds, especially striking in PRF 570 and 753.

Despite dealiasing deficiencies or failure and biases in flight speeds, flight directions could still be close to the actual directions in all PRF modes, especially if the main velocity sine curve happens to be still well discernible. In Figure 6, one can imagine that the main untreated velocity curve may peak in the same area as the fit from the wave plot and thus may ascertain the actual direction. The accuracy of such sine fits is unfortunately highly unreliable, though, as can be seen from Figure 12. Consequently, again, quality in the lowest PRF modes, especially 570, but also 753 and 1130, was rather poor and seasonal directional patterns were haphazard.

4.1.2. Insects

Overall, the HL dealiasing approach succeeded in insect cases given the lower flight speeds, lower variability and thus simpler radial velocity patterns. After dealiasing all PRF modes provided similar flight speeds and directions.

4.2. Dual PRF

4.2.1. Birds

Even though the main dual-PRF sine curves were not aliased, sidebands of outliers could be folded, which affected sine fit quality and derived data products. Two types of biases arose from outliers or outlier sidebands in dual PRF. A minor bias developed from the number of outliers. In bird cases, even though mean outlier proportion was 30%, i.e., twice as high as the 15% found by [18], in some cases, outliers could constitute almost 80% of all radial velocity measurements. Contrary to [18], thorough inspection showed that bird outlier removal is not mandatory given their symmetrical abundant allocation around the main curve (Figure 3), which does not impair sine fits. In simulations, increasing outlier proportions resulted in only a slight decrease in flight speeds. A major bias originated from aliased outliers which could lead to a reduction in flight speeds of up to 18 m s^{-1} in the VAD technique. Even though the aliasing of sidebands (with different amounts of outliers) occurred in a minority of migration events (20%), it is imperative to correct it as it can severely distort the model fit. Strong migration is typically associated with tailwinds which increase birds' ground speed and consequently the risk for aliasing and poor model fit. Poor model fit typically decreases flight speeds as could be also observed in our PRF comparisons. A threshold distance of 10 m s^{-1} from the first fit for outlier removal as in [18] can eliminate parts of the main sine curve and retain parts of sidebands biasing velocity products as deducible from Figure 5. Aliasing risk naturally varies with the dual-PRF Nyquist velocity, which was 48 m s^{-1} in the present study but can be considerably lower, e.g., 39.9 m s^{-1} in [25]. Lower dual-PRF Nyquist velocities are more prone to outlier aliasing, but this was not further assessed in the present work.

4.2.2. Insects

The outlier proportion in insect cases was much smaller than in bird cases (4% vs. 30%) and there was no aliasing in insect outliers. Standard deviations increase through mesoscale variability in wind fields such as gust fronts, sea-breeze fronts and roll vortices [39,40] where insects accumulate.

4.2.3. Precipitation

The outlier proportion in precipitation was only 0.7% and thus comparable to the proportions found by [25]. While widespread rain exhibited a mean residual standard deviation of 1.69 m s^{-1}, convective precipitation had a mean residual standard deviation of 3.45 m s^{-1}. In vol2bird, the option to use the correlation coefficient RhoHV could help improve outcomes at least in polarimetric radars, though caution is advised with certain overlap of polarimetric bird and insect characteristics with precipitation.

In summary, dual-PRF measurements regularly contained outliers of the measured radial velocity especially in birds, but also insects and precipitation. Outliers generally increased radial velocity standard deviations as in [18]. Dual-PRF standard deviations may work as a filter in single-polarisation radars similar to the vol2bird threshold of 2 m s^{-1} for single PRF.

4.3. Comparison of Dual PRF FMI vs. Single PRF in vol2bird

The intermediate to strong correlation between the MTRs of the FMI dual-PRF methodology and single PRF in vol2bird between 0–1 km could be interpreted as a positive sign that the methodologies produce similar outcomes. However, when looking at the underlying velocity and density data, the correlation analysis is misleading.

The comparison of single- and dual-PRF MTRs did not consistently reveal higher MTRs in dual PRF as one would expect. For correct interpretation, it is important to disentangle the different contributors to the MTRs.

Single-PRF flight speeds were mostly smaller than the dual PRF-based flight speeds; in the Utajärvi example, about 20–60%. However, dual-PRF velocities were collected only from one scan elevation, whereas single-PRF velocities were obtained from six elevations yielding more range bins for the VAD fit per height level. It would be reasonable to assume that if radial velocities were collected from several dual-PRF elevations, more height levels would contribute to MTRs and thus increase their magnitude, provided that enough bird bins are identified. Furthermore, the selection process for radial velocities differs between the methods. In the FMI approach, echo classification happens binwise prior to and apart from the radial velocity processing [4], while vol2bird uses the radial velocity as a layer-based filter. Blending velocity data from single PRF 570 passed through the HL algorithm and dual-PRF velocities in a VVP approach did not produce usable outcomes and is therefore discouraged.

As a further component of MTRs, bird densities were on average higher in vol2bird compared to the FMI method, which we attribute again to the identification of bird bins. The layer-based classification of vol2bird therefore potentially overestimates bird densities, while the FMI approach may under- to overestimate bird densities. As a result, MTRs obtained through the vol2bird algorithm can be higher than those from the FMI methodology despite faulty flight speeds from failed dealiasing and removal of low bird densities in vol2bird.

Our study did not involve directional information in the MTR calculations. However, considering the random patterns observed in the vol2bird flight directions compared to the more homogenous directions in dual PRF, it can be concluded that bias in MTRs will be aggravated when applying the alternative directional MTR equation. Bias will also affect other applications using single-PRF directions, as, e.g., in the separation of birds and insects (e.g., [41]) relying on correct flight speeds and directions.

A challenge in recognizing aliasing biases in processed bird profile data may be due to partly reasonable-looking flight directions (the phase of the sine curve) despite poor aliasing correction. Discrepancies emerge rather in flight speeds (amplitude) and the speed-dependent MTRs. Too small MTRs can be easily attributed to the low sensitivity of radars (resulting in low reflectivity). Reference outputs from alternative methodologies for WRs, which could help expose flaws, have been missing until recently. The calculation of MTRs makes them by definition prone to significant bias either from radial velocities or density calculations. For unknown reasons, the performance of the HL algorithm was not scrutinized despite WR calibration studies, e.g., [18]. For example, in [8], differences in MTRs between radar types were attributed to topography or different sample techniques by radars (vertical vs. quasi-horizontal), which can doubtlessly contribute to different bird numbers across areas. Likewise, the large-scale analyses by [20,42] deployed data from different kinds of single- and dual-PRF modes, including Finnish single-PRF data, without suspecting inherent velocity biases. Velocity bias is a strong explanatory candidate for the lower MTR rates in multi-radar studies between WRs or WRs and other radar systems.

To the best of our knowledge, there is currently no single-PRF algorithm available to disentangle the jumbled radial velocities in heavily aliased cases. Our results thus discourage the use of data from PRFs in the range of our lowest two modes. A challenge with accessing dual-PRF data can be that it is not necessarily shared through OPERA and it may be collected only from a few elevation angles. As per writing (4 November 2024), from the radar information from OPERA on the EUMETNET website [43], one can deduce that most of the operational single-PRF scan modes of European C-band WRs are executed in

ranges of 300–600 Hz, i.e., in the critical range with no prospects for successful dealiasing as shown here for PRF 570 Hz. Moreover, there is no standard dual-PRF methodology for biological analyses addressing the biases through (aliased) dual-PRF outliers and sidebands. Findings from the present study can help develop such.

5. Conclusions

Our study showed that firstly VAD-derived flight directions, flight speeds and consequently migration traffic rates from operational measurements in the common single-PRF range of C-band weather radars are unreliable and they typically grossly bias bird migration observations. Secondly, effective dealiasing is likewise essential for all echo types and for dual-PRF observations. Given the variability in WR systems and settings, an omnipotent dealiasing solution may be hard to find. One pivotal point is that dealiasing algorithms have been developed for precipitation, which typically exhibits more homogeneous radial velocity patterns than birds. Biological weather radar applications need to be built upon characteristics of biological entities and dedicated components. Otherwise, large-scale or long-term radar analyses could contain substantial biases which would falsify spatiotemporal biological products. It may be also advisable to check the validity of existing literature in the face of the present findings. Understanding aliasing patterns in both meteorological and non-meteorological Doppler velocity measurements helps improve radar data products in all fields of application. Appropriate velocity processing is imperative to strengthen the role of aeroecological research and WR applications.

Supplementary Materials: The following supporting information can be downloaded at: https://www.mdpi.com/article/10.3390/rs17030436/s1, Figure S1. Horizontal cross section of the interleaved single-PRF bird probabilities; Figure S2. Ground speeds for insects from untreated and dealiased velocities in 2023 and 2024; Figure S3. Comparison of migration traffic rates of the single-PRF and dual-PRF methodologies in 2022; Figure S4. Comparison of migration traffic rates of the single-PRF and dual-PRF methodologies in 2023 and 2024; Table S1. Mean ground speeds from the Utajärvi radar derived from single PRF and dual PRF.

Author Contributions: Conceptualization, N.W. and J.K.; methodology, N.W. and J.K.; validation, N.W. and J.K.; formal analysis, N.W.; writing—original draft preparation, N.W.; writing—review and editing, N.W., B.H. and J.K.; visualization, N.W. and B.H.; supervision, J.K.; project administration, N.W.; funding acquisition, N.W. All authors have read and agreed to the published version of the manuscript.

Funding: This research was partly funded through the HiRAD project from the 2022–2023 Biodiversa+ BiodivMon call for research proposals, with the funding organisations Swiss National Science Foundation (SNF 31BD30_216840), Belgian Federal Science Policy Office (BelSPO RT/24/HiRAD), Netherlands Organisation for Scientific Research (NWO EP.1512.22.003), and Academy of Finland (aka 359864).

Data Availability Statement: The original contributions presented in this study are included in the article/Supplementary Material. Further inquiries can be directed to the corresponding author. Data from the customized single-PRF and dual-PRF analyses can be downloaded from Zenodo. https://doi.org/10.5281/zenodo.14021462. Vol2bird data tables are available from the Aloft repository https://aloftdata.eu/, accessed on 29 June 2024.

Acknowledgments: We thank the anonymous reviewers for their valuable feedback on the manuscript. Furthermore, we extend our gratitude to Harri Hohti and Mikko Kurri for technical assistance with the customized PRF measurements and for sharing their valuable knowhow.

Conflicts of Interest: The authors declare no conflicts of interest. The funders had no role in the design of the study; in the collection, analyses, or interpretation of data; in the writing of the manuscript; or in the decision to publish the results.

Appendix A

Gaussian simulator of radial velocity measurements of birds

The radial Doppler velocity (V_r) measured from birds at height h, when the antenna is pointing at an elevation angle α, depends on the ground speed of birds, V_g, and on the climb rate of birds W_b. If β is the azimuth angle of the antenna with respect to the upwind motion of the ground speed, the Doppler velocity is given by

$$V_r = V_g \cos\alpha \cos\beta + W_b \sin\alpha \quad \text{(A1)}$$

Naturally, the ground velocity vector (V_g) of birds originates from the vector sum of birds' air speed V_b and horizontal downwind velocity V_h. Here, we use bold font for vectors and normal font for scalars. Note that the direction of downwind velocity deviates 180° from the usual meteorological concept of wind direction. For later use we specify V_g with its two scalar components: ground speed V_g and downwind direction of V_g, dir(V_g). Recognizing that elevation angles in the scans that are used for quantitative estimation of birds are commonly 0–10°, and that the average climb rate of, e.g., nocturnal passerines within the sample bin is less than 1–2 m s^{-1} [44], and that typical ground speeds of birds are in the range of 8–30 m s^{-1} [27] we can neglect the second term in Equation (A1). When bird motion is uniform at the height of interest (h) the first term as the function of azimuth angle will appear as the familiar sine curve (VAD) discussed in the main text of this paper.

Birds' radial velocity measurements contain high variability because of natural variation in birds' flight speed and directions and spatiotemporal variation in radar samples by elevation and azimuth. Consequently, velocity variance of migrating bird samples increases beyond that of widespread precipitation. The result is a randomly varying transient perturbation component in the measured radial velocity in neighbouring range bins and in the time series from a single bin.

Taking this variation into account, we generated a simulator for radial single and dual PRF-based velocities in a VAD-display. According to the first term of Equation (A1) on the right we set the height layer, the elevation angle and the ground speed vector of birds and obtain the average of V_r in each azimuth angle. When we calculate random samples of the radial Doppler velocity, V_{rs}, the simulator adds to the average ground speed vector a random perturbation vector V_g' that has a two-dimensional Gaussian distribution, namely consisting of velocity offset vel(V_g') and orientation offset dir(V_g'), notated as

$$\text{vel}(V_g') \sim N(0, \sigma^2 V_g') \quad \text{(A2)}$$

$$\text{dir}(V_g') \sim N(0, \sigma^2 \text{dir}(V_g')) \quad \text{(A3)}$$

which denote that both offsets are normally distributed, their expectation values are zero and their variances are the schematic σ^2 expressions on the right. In practice, we applied the following values when specifying the variance distributions, respectively: $\sigma^2 V_g' = (2 \text{ m s}^{-1})^2$, and $\sigma^2 \text{dir}(V_g') = (10°)^2$ resulting in the simulated ground velocity vector sample (V_{gs}):

$$V_{gs} = V_g + V_g' \quad \text{(A4)}$$

Finally, the respective simulated Doppler velocity sample (V_{rs}) is obtained from Equation (A1) assuming $W_b = 0$. Samples of V_{gs} (and outlier velocities) and respective estimates are randomly generated in each azimuth angle. V_{rs} values are displayed as a sine curve of dots in the VAD.

If a simulated radial velocity value is outside the respective Nyquist velocity range ($\pm V_{max}$) in either single- or dual-PRF simulation, it is shifted, i.e., aliased, according to

its magnitude to the respective aliased location corresponding to either single or two-fold aliasing of the PRF in question.

To generate outliers for the sidebands of the dual-PRF simulations, the desired proportion of simulated velocity data points destined to be outliers is randomly shifted by either ± 23.85 or ± 31.80, which is twice the unambiguous velocity of the low (900 Hz) and high (1200 Hz) PRF [25], respectively, constituting the dual-PRF measurements. In dual-PRF measurements this velocity error is more variable than in our simulation, but we chose this approach for simplicity, and it suffices to demonstrate the impact of the outliers on sine fits.

Applying these procedures yields Figure 1 for single PRF and Figure 9 for dual PRF.

References

1. Chilson, P.B.; Frick, W.F.; Stepanian, P.M.; Shipley, J.R.; Kunz, T.H.; Kelly, J.F. Estimating animal densities in the aerosphere using weather radar: To Z or not to Z? *Ecosphere* **2012**, *3*, 1–19. [CrossRef]
2. Dokter, A.M.; Desmet, P.; Spaaks, J.H.; van Hoey, S.; Veen, L.; Verlinden, L.; Nilsson, C.; Günther Haase, G.; Leijnse, H.; Farnsworth, A.; et al. bioRad: Biological analysis and visualization of weather radar data. *Ecography* **2019**, *42*, 852–860. [CrossRef]
3. Gauthreaux, S.A.; Diehl, R. Discrimination of biological scatterers in polarimetric weather radar data: Opportunities and challenges. *Remote Sens.* **2020**, *12*, 545. [CrossRef]
4. Mäkinen, T.; Ritvanen, J.; Pulkkinen, S.; Weisshaupt, N.; Koistinen, J. Bayesian classification of non-meteorological targets in polarimetric Doppler radar measurements. *J. Atmos. Ocean. Technol.* **2022**, *39*, 1561–1578. [CrossRef]
5. Gauthreaux, S.A. A radar and direct visual study of passerine spring migration in southern Louisiana. *Auk* **1971**, *88*, 343–365. [CrossRef]
6. Fischer, R.A.; Gauthreaux, S.A., Jr.; Valente, J.J.; Guilfoyle, M.P.; Kaller, M.D. Comparing transect survey and WSR-88D radar methods for monitoring daily changes in stopover migrant communities. *J. Field Ornithol.* **2012**, *83*, 61–72. [CrossRef]
7. Farnsworth, A.; Gauthreaux, S.A., Jr.; Blaricom, D.V. A comparison of nocturnal call counts of migrating birds and reflectivity measurements on Doppler radar. *J. Avian Biol.* **2004**, *35*, 365–369. [CrossRef]
8. Liechti, F.; Aschwanden, J.; Blew, J.; Boos, M.; Brabant, R.; Dokter, A.M.; Kosarev, V.; Lukach, M.; Maruri, M.; Reyniers, M.; et al. Cross-calibration of different radar systems for monitoring nocturnal bird migration across Europe and the Near East. *Ecography* **2019**, *42*, 887–898. [CrossRef]
9. Saltikoff, E.; Friedrich, K.; Soderholm, J.; Lengfeld, K.; Nelson, B.; Becker, A.; Hollmann, R.; Urban, B.; Heistermann, M.; Tassone, C. An overview of using weather radar for climatological studies: Successes, challenges, and potential. *Bull. Am. Meteorol. Soc.* **2019**, *100*, 1739–1752. [CrossRef]
10. Weisshaupt, N.; Lehtiniemi, T.; Koistinen, J. Combining citizen science and weather radar data to study large-scale bird movements. *IBIS* **2021**, *163*, 728–736. [CrossRef]
11. Saltikoff, E.; Haase, G.; Delobbe, L.; Gaussiat, N.; Martet, M.; Idziorek, D.; Leijnse, H.; Novák, P.; Lukach, M.; Stephan, K. OPERA the radar project. *Atmosphere* **2019**, *10*, 320. [CrossRef]
12. Desmet, P.; Shamoun-Baranes, J.; Kranstauber, B.; Dokter, A.M.; Weisshaupt, N.; Schmid, B.; Bauer, S.; Haase, G.; Bart Hoekstra, B.; Huybrechts, P.; et al. Biological data derived from European weather radars. *Sci. Data*, 2025; *in revision*.
13. Waldteufel, P.; Corbin, H. On the analysis of single-Doppler radar data. *J. Appl. Meteorol.* **1978**, *18*, 532–542. [CrossRef]
14. Holleman, I. Quality Control and Verification of Weather Radar Wind Profiles. *J. Atmos. Ocean. Technol.* **2005**, *22*, 1541–1550. [CrossRef]
15. Lhermitte, R.M.; Atlas, D. Precipitation motion by pulse Doppler Radar. In Proceedings of the Ninth Weather Radar Conference, Kansas City, MO, USA, 23–26 October 1961; pp. 218–223.
16. Browning, K.A.; Wexler, R. The determination of kinematic properties of a wind field using Doppler radar. *J. Appl. Meteorol. Climatol.* **1968**, *7*, 105–113. [CrossRef]
17. Press, W.H.; Teukolsky, S.A.; Vetterling, W.T.; Flannery, B.P. *Numerical Recipes in C: The Art of Scientic Computing*, 2nd ed.; Cambridge University Press: New York, NY, USA, 1992; p. 994.
18. Dokter, A.M.; Liechti, F.; Stark, H.; Delobbe, L.; Tabary, P.; Holleman, I. Bird migration flight altitudes studied by a network of operational weather radars. *J. R. Soc. Interface* **2010**, *8*, 30–43. [CrossRef] [PubMed]
19. Dokter, A.M.; Farnsworth, A.; Fink, D.; Ruiz-Gutierrez, V.; Hochachka, W.M.; La Sorte, F.A.; Robinson, O.J.; Rosenberg, K.V.; Kelling, S. Seasonal abundance and survival of North America's migratory avifauna determined by weather radar. *Nat. Ecol. Evol.* **2018**, *2*, 1603–1609. [CrossRef]
20. Nilsson, C.; Dokter, A.M.; Verlinden, L.; Shamoun-Baranes, J.; Schmid, B.; Desmet, P.; Bauer, S.; Chapman, J.; Alves, J.A.; Stepanian, P.M.; et al. Revealing patterns of nocturnal migration using the European weather radar network. *Ecography* **2018**, *42*, 876–886. [CrossRef]

21. Rosenberg, K.V.; Dokter, A.M.; Blancher, P.J.; Sauer, J.R.; Smith, A.C.; Smith, P.A.; Stanton, J.C.; Panjabi, A.; Helft, L.; Parr, M.; et al. Decline of the North American avifauna. *Science* **2019**, *366*, 120–124. [CrossRef]
22. Feldmann, M.; James, C.N.; Boscacci, M.; Leuenberger, D.; Gabella, M.; Germann, U.; Wolfensberger, D.; Berne, A. R2D2: A Region-Based Recursive Doppler Dealiasing Algorithm for Operational Weather Radar. *J. Atmos. Ocean. Technol.* **2020**, *37*, 2341–2356. [CrossRef]
23. Bergen, W.R.; Albers, S.C. Two- and three-dimensional de-aliasing of Doppler radar velocities. *J. Atmos. Ocean. Technol.* **1988**, *5*, 305–319. [CrossRef]
24. Wüest, M.; Germann, U.; Schmid, W. A variational de-aliasing technique. *Phys. Chem. Earth Part B Hydrol. Oceans Atmos.* **2000**, *25*, 1179–1183. [CrossRef]
25. Holleman, I.; Beekhuis, H. Analysis and correction of dual PRF velocity data. *J. Atmos. Ocean. Technol.* **2003**, *20*, 443–453. [CrossRef]
26. Weisshaupt, N.; Koistinen, J. Dealiasing of radial velocities based on interleaved dual-PRF measurements and bin-based polarimetric echo classification. In Proceedings of the 3rd International Radar Aeroecology Conference, Davos, Switzerland, 25–26 June 2022.
27. Bruderer, B.; Boldt, A. Flight characteristics of birds: I. Radar measurements of speeds. *IBIS* **2001**, *143*, 178–204. [CrossRef]
28. Battan, L.J. *Radar Observation of the Atmosphere*; The University of Chicago Press: Chicago, IL, USA; London, UK, 1973; 324p.
29. Haase, G.; Landelius, T. Dealiasing of Doppler Radar Velocities Using a Torus Mapping. *J. Atmos. Ocean. Technol.* **2004**, *21*, 1566–1573. [CrossRef]
30. Joe, P.; May, P.T. Correction of Dual PRF Velocity Errors for Operational Doppler Weather Radars. *J. Atmos. Ocean. Technol.* **2003**, *20*, 429–442. [CrossRef]
31. Dazhang, T.; Geotis, S.G.; Passarelli., R.E., Jr.; Hansen, A.L.; Frush, C.L. Evaluation of an alternating-PRF method for extending the range of unambiguous Doppler velocity. In Proceedings of the 22nd Conference on Radar Meteorology, Zurich, Switzerland, 10–13 September 1984; American Meteorological Society: Boston, MA, USA, 1984; pp. 523–527.
32. Jorgensen, D.P.; Shepherd, T.R.; Goldstein, A.S. A Dual-Pulse Repetition Frequency Scheme for Mitigating Velocity Ambiguities of the NOAA P-3 Airborne Doppler Radar. *J. Atmos. Ocean. Technol.* **2000**, *17*, 585–594. [CrossRef]
33. Altube, P.; Bech, J.; Argemí, O.; Rigo, T.; Pineda, N.; Collis, S.; Helmus, J. Correction of Dual-PRF Doppler Velocity Outliers in the Presence of Aliasing. *J. Atmos. Ocean. Technol.* **2017**, *34*, 1529–1543. [CrossRef]
34. Achtemeier, G.L. The Use of Insects as Tracers for "Clear-Air" Boundary-Layer Studies by Doppler Radar. *J. Atmos. Ocean. Technol.* **1991**, *8*, 746–765. [CrossRef]
35. Wainwright, C.E.; Stepanian, P.M.; Reynolds, D.R. The movement of small insects in the convective boundary layer: Linking patterns to processes. *Sci. Rep.* **2017**, *7*, 5438. [CrossRef]
36. Tabary, P.; Scialom, G.; Germann, U. Real-time retrieval of the wind from aliased velocities measured by Doppler radars. *J. Atmos. Ocean. Technol.* **2001**, *18*, 875–882. [CrossRef]
37. Van Rossum, G.; Drake, F.L. *Python 3 Reference Manual*; CreateSpace: Scotts Valley, CA, USA, 2009.
38. R Core Team. *R: A Language and Environment for Statistical Computing*; R Foundation for Statistical Computing: Vienna, Austria, 2023; Available online: https://www.R-project.org/ (accessed on 1 October 2024).
39. Etling, D.; Brown, R.A. Roll vortices in the planetary boundary layer: A review. *Bound-Layer Meteorol.* **1993**, *65*, 215–248. [CrossRef]
40. Geerts, B.; Miao, Q. Airborne Radar Observations of the Flight Behavior of Small Insects in the Atmospheric Convective Boundary Layer. *Environ. Entomol.* **2005**, *34*, 361–377. [CrossRef]
41. Nussbaumer, R.; Schmid, B.; Bauer, S.; Liechti, F. A Gaussian Mixture Model to Separate Birds and Insects in Single-Polarization Weather Radar Data. *Remote Sens.* **2021**, *13*, 1989. [CrossRef]
42. Nussbaumer, R.; Benoit, L.; Mariethoz, G.; Liechti, F.; Bauer, S.; Schmid, B. A Geostatistical Approach to Estimate High Resolution Nocturnal Bird Migration Densities from a Weather Radar Network. *Remote Sens.* **2019**, *11*, 2233. [CrossRef]
43. EUMETNET. Available online: https://www.eumetnet.eu/activities/observations-programme/current-activities/opera/ (accessed on 12 November 2024).
44. Liechti, F.; Bauer, S.; Dhanjal-Adams, K.L.; Emmenegger, T.; Zehtindjiev, P.; Hahn, S. Miniaturized multi-sensor loggers provide new insight into year-round flight behaviour of small trans-Sahara avian migrants. *Mov. Ecol.* **2018**, *6*, 19. [CrossRef]